Trifluoroacetic acid deposition from emissions of HFO-1234yf in India, China, and the Middle East

Liji M. David[*1,2], Mary Barth[*3], Lena Höglund-Isaksson[4], Pallav Purohit[4], Guus J. M. Velders[5,6], Sam Glaser[1,7], and Akkihebbal. R. Ravishankara[*1,2]

[1]Department of Chemistry, Colorado State University, Fort Collins, CO 80523, USA
[2]Department of Atmospheric Science, Colorado State University, Fort Collins, CO 80523, USA
[3]Atmospheric Chemistry Observations and Modeling Laboratory, National Center for Atmospheric Research, Boulder, Colorado
[4]Air Quality and Greenhouse Gases Program, International Institute for Applied Systems Analysis (IIASA), Schlossplatz 1, 2361, Laxenburg, Austria
[5]National Institute for Public Health and the Environment (RIVM), PO Box 1, 3720 BA Bilthoven, The Netherlands
[6]Institute for Marine and Atmospheric Research Utrecht, Utrecht University, The Netherlands
[7]Currently at Tufts University, Medford, MA

Address correspondence to: liji.david@usu.edu, barthm@ucar.edu, and a.r.ravishankara@colostate.edu

Key points

1. The expected concentrations of trifluoroacetic acid (TFA) from the degradation of HFO-1234yf ($CF_3CF=CH_2$) emitted now and in the future by India, China, and the Middle East were calculated using GEOS-Chem and WRF-Chem models.
2. We conclude that, with the current knowledge of the effects of TFA on humans and ecosystems, the projected emissions through 2040 would not be detrimental.
3. We carried out various tests and conclude that the model results are robust.
4. The major uncertainty in the knowledge of the TFA concentrations and their spatial distributions is due to uncertainties in the future projected emissions.

Abstract

We have investigated trifluoroacetic acid (TFA) formation from emissions of HFO-1234yf, its dry and wet deposition, and rainwater concentration over India, China, and the Middle East with GEOS-Chem and WRF-Chem models. We estimated the TFA deposition and rainwater concentrations between 2020 and 2040 for four previously published HFO-1234yf emission scenarios to bound the possible levels of TFA. We evaluated the capability of GEOS-Chem to capture the wet deposition process by comparing calculated sulfate in rainwater with observations. Our calculated TFA amounts over the U.S., Europe, and China were comparable to those previously reported when normalized to the same emission. A significant proportion of TFA was found to be deposited outside the emission regions. The mean and the extremes of TFA rainwater concentrations calculated for the four emission scenarios from GEOS-Chem and WRF-Chem were orders of magnitude below the no observable effect concentration. The ecological and human health impacts now and continued use of HFO-1234yf in India, China, and the Middle East are estimated to be insignificant based on the current understanding, as summarized by Neale et al. (2021).

Keywords: HFO-1234yf, Trifluoroacetic acid, wet and dry deposition, India, China, the Middle East.

1. **Introduction**

The use of olefinic hydrofluorocarbons (HFCs) as substitutes for HFC-134a (1,1,1,2-tetrafluoroethane, CF_3CFH_2) are increasing in both the developed and developing countries (Velders et al., 2009). HFC-134a is a replacement for chlorofluorocarbons (CFCs) and hydrochlorofluorocarbons (HCFCs), which were phased out under the Montreal Protocol and its many amendments and adjustments (WMO/UNEP Quadrennial Ozone Layer Assessment, 2007). HFC-134a is a potent greenhouse gas with a 100-year global warming potential (GWP) of 1600 (Hodnebrog et al., 2020). HFO-1234yf (2,3,3,3-tetrafluoropropene, $CF_3CF=CH_2$) with a 100-year GWP of <1 (IPCC report (Myhre et al., 2013)) is a replacement for HFC-134a in automobile air conditioners (MAC) (Papadimitriou et al., 2008). The atmospheric degradation of HFO-1234yf leads to trifluoro acetyl fluoride ($CF_3C(O)F$) (Young and Mabury, 2010). $CF_3C(O)F$ hydrolyzes rapidly to yield trifluoroacetic acid (TFA, $CF_3-C(O)OH$), which is removed from the atmosphere by dry and wet deposition (George et al., 1994). The chemical lifetime of HFC-134a (~14 years) is such that it is reasonably well-mixed globally upon emission into the atmosphere. Therefore, its degradation and the TFA formed will occur across the globe. Only about 30% of the emitted HFC-134a leads to TFA (Kotamarthi et al., 1998). Other research (Wallington et al., 1996) shows that hot $CF_3C(O)FH$ formed in the degradation scheme would significantly reduce the TFA yield from HFC-134a. This reduction is not explicitly considered here, but we acknowledge that the noted TFA yields from HFC-134a can be viewed as upper limits. A large fraction of the formed TFA is deposited into the oceans. The fraction of HFC-134a degraded per year from one year's emission would be small, leading to small TFA in rainwater concentrations at a given location. However,

as HFC-134a accumulates in the atmosphere, more TFA would be produced. HFO-1234yf has a shorter chemical lifetime of a few (~10) days (Myhre et al., 2013) and its degradation leads almost exclusively (~100%) to $CF_3C(O)F$. Therefore, TFA deposition per year of emission will be higher, depending on the year, and more localized spatially.

Previous studies have focused on TFA formation from emissions of either HFC-134a at the current or previous levels (Kanakidou et al., 1995; Kotamarthi et al., 1998) or HFO-1234yf substituted for current levels of HFC-134a usage (Luecken et al., 2010); then, they have mostly scaled it for scenarios of HFO-1234yf emissions in the future over the continental U.S. and Europe (Henne et al., 2012; Papasavva et al., 2009). Some works have distinguished between uses of HFC-134a in MAC versus total usage, while others have evaluated maximum use scenarios. These studies suggest that toxic levels of TFA in water bodies are not produced over Europe, North America, and China if HFO-1234yf replaces all the current use of HFC-134a (Henne et al., 2012; Kazil et al., 2014; Luecken et al., 2010; Wang et al., 2018). Russell et al. (2012) conducted a model study to determine TFA concentration in terminal water bodies in the contiguous U.S., with TFA deposition rates from Luecken et al. (2010). They found that after 50 years of continuous emissions, aquatic concentrations of 1 to 15 $\mu g\ L^{-1}$ are projected, with extreme concentrations of up to 50 to 200 $\mu g\ L^{-1}$ in the arid southwestern U.S.

Kazil et al. (2014) investigated, using the WRF-Chem model, the atmospheric turnover time of HFO-1234yf, the dry and wet deposition of TFA, and the TFA rainwater concentration over the contiguous U.S. between May and September 2006. They also examined where TFA deposited emissions of three specific regions in the U.S. They concluded that the average TFA rainwater concentration was 0.89 $\mu g\ L^{-1}$ for the contiguous U.S. Although Kazil et al. (2014) used emissions twice as large as that used by Luecken et al. (2010), the TFA rainwater concentrations were comparable. Kazil et al. (2014) used the measured HFC-134a to CO ratio from the Los Angeles area to obtain potential HFO-1234yf emissions. They also showed that TFA rainwater concentrations reached significantly higher values (7.8 $\mu g\ L^{-1}$) at locations with very low precipitation on shorter time scales. A comparably low TFA wet deposition occurred in the dry western U.S. The work of Wang et al. (2018) is similar to that of Henne et al. (2012) and used the GEOS-Chem model and examined the rainwater content and deposited amounts of TFA over Europe, the U.S, and China, with similar findings. Henne et al. (2012) is the only study that used two different models (FLEXPART and STOCHEM) to study the TFA deposition and rainwater concentration over Europe.

The above-noted studies focused on the U.S. and Europe, and most recently China. The U.S. and Europe emissions of the sum of HFC-134a and HFO-1234yf are expected to increase only in proportion to the population in the future since the per capita number of MAC, stationary AC, and other cooling units are unlikely to increase rapidly. India, China, and the Middle East are the regions with expected large increases in HFO-1234yf use. In these regions, the number of units and associated usage will increase rapidly as the economies grow. Perhaps Latin America and parts of Africa would also see similar increases. The above-noted studies from the U.S. and Europe do not allow us to draw firm conclusions about TFA's formation from realistic future emissions from

Asia (China and the Indian subcontinent), where the markets are not saturated, and meteorology is very different from North America and Europe. The rate of degradation of parent compounds and precipitation will differ in the warmer tropical and subtropical regions from those seen for the U.S. and Europe; the seasonality will also be different. The precipitation across Asia is associated with the Asian monsoon, which is stronger in comparison to the monsoon in the southwest U.S. It is also essential to look at the Middle East emissions since the studies of Kazil et al. (2014) and Russell et al. (2012) showed that TFA rainwater concentrations are larger over drier areas of the U.S., and there can be more accumulation in arid regions.

In 2019 the Kigali Amendment to the Montreal Protocol went into force. According to the amendment the production and use of HFCs has to be phased down in the coming decades. This should reduce the emissions of HFCs such as HFC-134a, but will likely increase emissions of HFO-1234yf.

A description of the models used (GEOS-Chem and WRF-Chem), HFO-1234yf emission scenarios, and the chemical scheme are given in section 2. In section 3, we compare the precipitation in GEOS-Chem and WRF-Chem with observations. We evaluate the GEOS-Chem model's ability to reproduce wet deposition by comparing sulfate rainwater concentrations with observations. We performed simulations using both the models for the three domains individually to calculate the TFA's dry and wet deposition and rainwater concentrations over India, China, and the Middle East. We performed two-year runs in GEOS-Chem to check for interannual variability. We compare our simulation results with other studies for the U.S., Europe, and China. The HFO-1234yf emissions from all the regions together were also simulated to assess the interregional effects. Major findings from this study are summarized in section 4.

2.   Methods
2.1.   Model description

GEOS-Chem: We used the GEOS-Chem (v12.0.3, www.geos-chem.org) global three-dimensional chemical transport model driven by GEOS-FP assimilated meteorological data. GEOS-Chem has a fully coupled tropospheric NO_x-O_x-hydrocarbon-aerosol chemistry. The simulations were made at 2°×2.5° resolution and 47 vertical levels from the surface to ~80 km. The wet deposition of aerosols and soluble gases by precipitation includes the scavenging in convective updrafts, in-cloud rainout, and below-cloud washout (Amos et al., 2012; Liu et al., 2001). The dry deposition was calculated using a resistance-in-series parameterization, which is dependent on environmental variables and lookup table values (Wesely, 1989). The simulations were conducted for 2015 and 2016 following a 2-month spin-up.

The global anthropogenic emissions were from Emissions Database for Global Atmospheric Research (version 4.3). The global emissions are superseded by regional emission inventories for India (Speciated Multi-pOllutants Generator (SMOG) and MIX) (Li et al., 2017; Pandey et al., 2014; Sadavarte and Venkataraman, 2014), China (MIX), Europe (EMEP), U.S. (National Emissions Inventory (NEI) 2011) (NEI2011, http://ww.epa.gov/air-emissions-inventories), Canada (Criteria Air Contaminants (CAC), http://www.ec.gc.ca/), and Mexico

151 (BRAVO) (Kuhns et al., 2005). We used the biomass burning from Global Fire Emissions
152 Database (GFED) version 4 (Giglio et al., 2013). The biogenic VOC emissions were from the
153 Model of Emissions of Gases and Aerosols from Nature (MEGAN) version 2.1 inventory of
154 Guenther et al (2012). The details on other emissions are described in David et al. (2018, 2019).
155 **WRF-Chem:** The Weather Research and Forecast with Chemistry (WRF-Chem) model (Fast et
156 al., 2006; Grell et al., 2005) version 4.1.3, was used to simulate meteorology and chemistry over
157 India, China, and the Middle East individually. The WRF-Chem simulations were integrated for
158 14 months, beginning 1 November 2014 and ending 31 December 2015, with the first two months
159 of the simulation was used to spin up the model chemistry. The three model domains, shown in
160 Figure 1, have a horizontal grid spacing of 30 km and 40 vertical levels reaching a model top of
161 50 hPa. The vertical levels stretch in size with a fine resolution near the surface and a coarser
162 resolution in the upper troposphere. The model meteorology was initialized with Global Forecast
163 System (GFS) archived at 0.5° and a temporal resolution of 6 hours. Observational nudging is
164 applied for temperature, moisture, and winds to keep large-scale features in line with the observed
165 meteorology. The model physics and chemistry options that were used are summarized in Table
166 S1 in the supplementary information. The Model for Ozone and Related chemical Tracers
167 (MOZART) gas-phase chemical mechanism and the Global Ozone Chemistry Aerosol Radiation
168 and Transport (GOCART) scheme for aerosols (MOZCART) (Pfister et al., 2011) were used to
169 simulate ozone and aerosol chemistry. TFA chemistry was added to this chemical option. Six-
170 hourly results from the Community Atmosphere Model with Chemistry (CAM-Chem), which has
171 a similar chemistry mechanism as the WRF-Chem model configuration, were used (Tilmes et al.,
172 2015) to initialize trace gas and aerosol mixing ratios as well as to provide lateral boundary
173 conditions. HFO-1234yf and TFA were initialized with the GEOS-Chem results described above.
174 The Model of Emissions of Gases and Aerosols from Nature (MEGAN v2.04; Guenther, 2007)
175 was used to represent the net biogenic emissions for both gases and aerosols. Anthropogenic
176 emissions were from the Emissions Database for Global Atmospheric Research – Hemispheric
177 Transport of Air Pollution (EDGAR-HTAP) emission inventory (Janssens-Maenhout et al., 2015).
178 The Fire Inventory from NCAR version 1 (FINNv1.6; Wiedinmyer et al., 2011) was implemented
179 to provide daily varying emissions of trace species from biomass burning.

180   The wet removal scheme in WRF-Chem for MOZART chemistry, based on Neu and
181 Prather (2012), was used to compute the dissolution of soluble trace gases into precipitation and
182 their release into the gas phase upon evaporation of hydrometeors. Neu and Prather (2012) estimate
183 trace gas removal by multiplying the effective Henry's law equilibrium aqueous concentration by
184 the net precipitation formation (conversion of cloud water to precipitation, minus evaporation of
185 precipitation). Dry deposition of trace gases was described with the Wesely (1989)
186 parameterization. Diagnostic information on the wet and dry deposition of TFA was determined
187 every time step and accumulated values were included in the output files.

188

189 **2.2.   Emissions**

190   HFO-1234yf is just now entering the market driven by regional (e.g., the European Union's
191 MAC Directive 2006/40/EC), national (e.g., Japan and U.S.) F-gas regulations, and the Kigali
192 Amendment to the Montreal Protocol. HFC-134a is currently the primary working fluid of MAC
193 and other applications (refrigerant, insulating foams, and aerosol propellants). Therefore, we have
194 to estimate the future emission levels from the three regions of interest. Unlike the developed
195 countries, India, China, and the Middle East are growing rapidly and the use of air conditioning
196 and refrigeration (and other uses of HFCs and HFOs) are expected to increase rapidly. Therefore,
197 one has to consider the likely economic growth and other factors in estimating emissions levels.
198 Here, we explore a few different potential scenarios for emissions of HFO-1234yf.
199   TFA production from HFO-1234yf increases linearly with the rise in HFO-1234yf
200 emissions, i.e., there is no feedback on this process since the primary drivers for the degradation
201 of this chemical, the OH radical, will not be altered by their relatively small emissions. In addition,
202 the changes in the abundance of OH in the troposphere in the next few decades are unlikely to be
203 different (say <13%) than the current levels based on the changes seen over the past few decades
204 (Rigby et al., 2017). Therefore, we can estimate the extent of TFA formation from a set of
205 modeling calculations that employed a fixed total amount of HFO-1234yf from each region. After
206 that, we can calculate the extent of TFA formation for various possible emission scenarios.
207   We used four future HFO-1234yf emissions scenarios for the 2020 to 2040 period: (1)
208 estimate of the upper range scenario HFO-1234yf emissions based on Velders et al. (2015)
209 estimate; (2) lower range scenario of HFO-1234yf based on Velders et al. (2015) estimate; (3) the
210 Greenhouse Gas Air Pollution Interactions and Synergies (GAINS) model (Amann et al., 2011)
211 with maximum technically feasible reduction (MTFR) estimates of HFO-1234yf; and (4) the
212 GAINS 'maximum HFO' (max HFO) scenario. Given the relatively short lifetime of HFO-1234yf,
213 the TFA production per year is dependent only on the emissions in that year. Figure 2 shows the
214 HFO-1234yf emission projection from India, China, and the Middle East for the four scenarios
215 between 2020 and 2040. The scenario based on Kumar et al. (2018) is similar to the fourth scenario
216 we considered. Therefore, we have not specifically included this possibility.
217   The emission estimates of HFO-1234yf in the GAINS model depends on when countries
218 will comply with the Kigali Amendment, current and future emissions based on country-level
219 activity data, uncontrolled emission factors, the removal efficiency of emission control measures,
220 and the extent to which such measures are applied (Purohit and Höglund-Isaksson, 2017). The
221 GAINS model uses the fuel input for the transport sector that is provided by the exogenous
222 projections (e.g., International Energy Agency's World Energy Outlook 2017). First, using the
223 annual mileage per vehicle (veh-km) and specific fuel consumption (SFC), GAINS estimates the
224 number of vehicles (by type, fuel). Second, using the penetration rate of a MAC, the number of
225 vehicles with MAC is calculated. Next, using the specific refrigerant charge (different for MAC
226 used in vehicle types), the HFO-1234yf consumption in mobile air conditioners is calculated. Note
227 that the HFO-1234yf is assumed to be substituted for HFC-134a, one-to-one, in all vehicles. For
228 HFO-1234yf use in MAC, HFO-1234yf emissions are estimated separately for "banked"
229 emissions, i.e., leakage from equipment in use, and for "scrapping" emissions, i.e., emissions

230   released at the end-of-life of the equipment. The leakage rate in the GAINS model assumes a
231   percentage of the charge per year. For example, if the refrigerant charge in MAC is 0.5 kg then the
232   emissions from the bank will be 0.05 kg (= 0.5 kg×0.1) per year, where the leakage rate is 10%
233   per year. This leakage rate is a steady refrigerant loss through seals, hoses, connections, valves,
234   etc. from every MAC over the entire use-phase (annually). At the end-of-life, the scrapped
235   equipment is assumed to be fully loaded with refrigerant, which needs recovery, recycling, or
236   destruction. At the same time, if there are regulations in place (e.g., MAC Directive 2006/40/EC
237   in European Union) - a package of measures including leak prevention during use and refill,
238   maintenance, and end of life recovery, and recollection of refrigerants, GAINS consider these good
239   practices as a control option with a removal efficiency of 50% for *in-use* and 80% for *end-of-life* -
240   based on secondary sources (Purohit et al., 2020). However, no such measures are assumed for
241   India, China, and the Middle East. Thus, these emissions can be considered the maximum likely
242   emissions. The MTFR version of the GAINS scenario assumes that the maximum technically
243   feasible reductions are applied across the sectors in India, China, and the Middle East. The Velders
244   et al. (2015) emissions also follow the Kigali amendment. The 'Shared Socioeconomic Pathways'
245   (SSPs) SSP3 and SSP5 are the lower and upper range scenarios, respectively, used in Velders et
246   al. (2015) calculated for 11 geographic regions and 13 use categories. Kumar et al. (2018) highlight
247   that many applications in India will likely transition to something other than HFOs. These trends
248   are not unique to India and will likely be replicated in China and the Middle East. Therefore, the
249   four HFO-1234yf emission scenarios for the 2020 to 2040 period represent emissions that are
250   higher than should be expected and, therefore, are upper limit estimates of the potential impact of
251   TFA in these regions.
252   To minimize numerical errors (in using small emissions) and compare them with previous
253   studies, we used HFO-1234yf emissions of ~40 Gg yr^{-1} from each of these regions. This value
254   corresponds to 2025 projected emissions from the GAINS model over India and the Middle East
255   if all the applications were to use HFO-1234yf in place of HFC-134a for China, the emission values
256   are for 2016 from Wang et al. (2018). Figure S1 in the supplementary information shows the annual
257   spatial distribution of HFO-1234yf over India, China, and the Middle East as simulated in: (i)
258   GEOS-Chem; and (ii) WRF-Chem models. We distributed this total emission across the
259   country/region of interest by scaling the emission to known anthropogenic CO emissions used in
260   the model. The anthropogenic CO is a good tracer for HFO-1234yf emissions since they originate
261   from similar applications (especially the transport sector) and in proportion to the distribution of
262   economic activities in the region/country of interest. We show the total emissions in each of the
263   three regions in both the models in the figure. The distribution varies to a small extent with the
264   season (shown in Figure S2 in the supplementary information), and the monthly variation in
265   emission is similar in both models. We also simulated GEOS-Chem over the US and Europe using
266   the total HFO-1234yf emissions from Wang et al. (2018) and Henne et al. (2012), respectively.
267
268   **2.3.   Chemical scheme**

269   The chemical degradation of HFO-1234yf and the production of TFA were added to both
270   the GEOS-Chem NO_x-O_x-hydrocarbon-aerosol chemistry scheme and the WRF-Chem
271   MOZCART chemistry scheme. The detailed chemical scheme for the formation of TFA from
272   HFO-1234yf is shown in Burkholder et al. (2015) and, therefore, not repeated here. The simplified
273   representation of TFA production follows that of Kazil et al. (2014):

275   $OH + CF_3CF = CH_2 \rightarrow CF_3C(O)F (gas\ phase)$ (1)

276   $CF_3C(O)F (gas\ phase) \rightarrow inclouds \rightarrow CF_3C(O)OH$ (2)

277   $CF_3C(O)F (clouds) \rightarrow Wet\ depostion$ (3)

278   $CF_3C(O)F (clouds) \rightarrow CF_3C(O)OH (gas\ phase)$ (4)

279   $CF_3C(O)OH (gas\ phase) + OH \rightarrow loss$ (5)

280   $CF_3C(O)OH (gas\ phase) \rightarrow dry\ deposition$ (6)
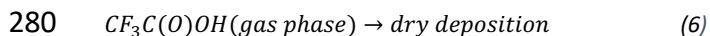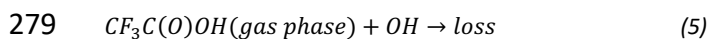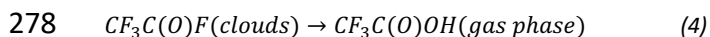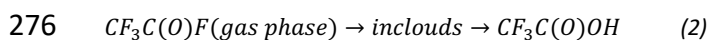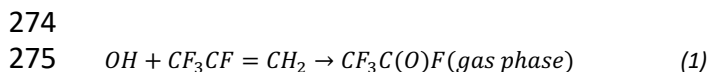
282   The conversion of HFO-1234yf to TFA includes OH-initiated reaction of $CF_3CF=CH_2$
283   (Equation 1) with a temperature-dependent rate coefficient of $1.26\times10^{-12} \exp(-35/T)$ cm^3 molecule$^-$
284   ^{1} s^{-1} to produce gas-phase $CF_3C(O)F$ (note that the initial OH reaction is the rate-limiting step in
285   the conversion). The gas-phase removal of $CF_3C(O)F$ is not rapid but hydrolyzes to TFA in water
286   (George et al., 1994) (Equation 2). The hydrolysis process is added to the heterogeneous chemistry
287   with a hydrolysis rate of 150 s^{-1}, and Henry's Law solubility constant of 3 M atm^{-1}. TFA is highly
288   soluble in cloud water. Upon cloud evaporation, the dissolved TFA is released into the gas phase
289   (Equation 4). The gas-phase TFA is expected to be deposited either via dry (Equation 6) or wet
290   deposition using Henry's Law solubility constant of 9×10^3 M atm^{-1} at a standard temperature of
291   298.15 K, $\Delta H/R = 9000$ K, dissociation coefficient of 0.65 mol L^{-1} at 298.15 K, and $\Delta E/R = -1562$
292   K. Thus, at cloud temperatures (generally <290 K) the effective Henry's Law of TFA is high,
293   characterizing TFA as a highly soluble gas. The dry deposition rate for TFA is assumed to be the
294   same as that for nitric acid (Henne et al., 2012; Kazil et al., 2014; Luecken et al., 2010). We also
295   included the potential loss of gas-phase TFA by its reaction with OH radicals (Equation 5) with a
296   rate coefficient of 9.35×10^{-14} cm^3 molecule^{-1} s^{-1}. Other potential losses of HFO-1234yf via reaction
297   with Cl, O_3, and NO_3 are very small and all yield the same set of products. Therefore, we have not
298   included them in the model. We also examined the possible removal of gas phase TFA by its
299   reaction with Criegee intermediate (CI). We used the Bristol group's calculated concentrations of
300   the Criegee intermediates (Chhantyal-Pun et al., 2017; Khan et al., 2018).

302   **3.   Results and Discussion**
303   **3.1.   Sulfate concentration in rainwater**
304   Wet deposition is one of the primary removal processes for TFA. This deposition depends
305   on precipitation amounts and how well our model captures the wet deposition process, making it
306   crucial to evaluate the models used here to capture these two factors.

307   First, we compared the annual total precipitation amounts calculated by GEOS-Chem and
308   WRF-Chem with the observed daily total accumulated precipitation from the Tropical Rainfall
309   Monitoring Mission (TRMM_3B42_daily product) in the three regions (Figure S3a in the
310   supplementary information). The TRMM product is at a 0.25º×0.25º resolution. The spatial
311   distribution of seasonal total precipitation in the three domains from the two models and TRMM
312   is shown in Figure S4 in the supplementary information. Both the models captured the seasonal
313   precipitation patterns. As seen in Figure S3a, the total precipitation amounts were a factor of 1.5-
314   2 higher in GEOS-Chem compared to WRF and TRMM. (The ratio of total precipitation between
315   GEOS-Chem and WRF-Chem(TRMM) were 2.6 (1.5), 2.2 (1.5), and 2.2 (1.4) for India, China,
316   and the Middle East, respectively). WRF-Chem underestimated the precipitation amounts
317   compared to TRMM in the three regions. Kumar et al. (2012; 2018) have addressed the
318   precipitation biases in WRF-Chem compared to TRMM over South Asia. We attribute the higher
319   precipitation in GEOS-Chem to: (a) the different model physics used; (b) the effects of a
320   meteorology-driven chemistry transport model (GEOS-Chem) versus an "online" chemistry
321   transport model (WRF-Chem) where chemistry is solved at the same time step as the meteorology;
322   (c) and to the different grid spacings used by the two models, noting that the coarse GEOS-Chem
323   grid cells contain several convective storms compared to that in WRF-Chem. The monthly
324   variation in total precipitation is shown in Figure S3b (supplementary information), and both
325   models have similar trends as that observed by TRMM.

326   To evaluate the accuracy of the TFA wet deposition, it is useful to compare sulfate wet
327   deposition amounts produced by the oxidation of SO_2. The emissions of SO_2 are comparable in
328   both the models (shown in Figure S5 in the supplementary information). We have measurements
329   of sulfate rainwater concentrations in some of the regions. Further, the lifetime of SO_2 in the
330   troposphere is comparable to that of HFO-1234yf. We hasten to add that while the HFO-1234yf
331   degradation is controlled by gas phase OH reactions, that of SO_2 includes both gas and condensed
332   phase processes. However, the removal of both sulfate and TFA are due to condensed phase
333   reactions. The WRF-Chem model has been shown to capture the sulfate rainwater concentration
334   over the continental U.S. by Kazil et al. (2014); we expect it to do well over this study's regions.
335   However, GEOS-Chem has not been evaluated previously. There are no networks for measuring
336   sulfate rainwater concentration in India and the Middle East. Yet, there are some observations of
337   rainwater sulfate in the published articles in all three domains. The available data are sparse, and
338   the observations for 2015 (the modeled year) are even fewer to make a comparison with WRF-
339   Chem simulations. However, GEOS-Chem simulations were available from our previous work for
340   2000-2015. We used those results to compare with observations during that period. The
341   observation locations (over land only) in the three domains are shown in Figure S6 in the
342   supplementary information. Figure 3 shows the scatter plot of simulated and observed sulfate
343   rainwater concentration in the three domains. Table 1 lists the statistics of the comparison between
344   GEOS-Chem and the observations. Rainwater sulfate amounts calculated by GEOS-Chem
345   correlate well (R>0.80) with observations. We see a bias of -13, -13, and -3% in India, China, and
346   the Middle East domains, respectively. The negative bias in GEOS-Chem sulfate rainwater

concentration could be because the model integrates over a large area while the observations are point locations. It could also be, as noted earlier, because GEOS-Chem yields higher amounts of precipitation and thus could lead to smaller rainwater concentrations. We suggest that these values are good to at least a factor of two. In summary, the GEOS-Chem model shows considerable skill in reproducing mean sulfate rainwater concentrations and spatial variability of sulfate rainwater concentrations; therefore, it can be utilized to calculate TFA wet deposition.

3.2. Comparison of calculated TFA with previous studies

Before presenting the results of the calculations for India, China, and the Middle East from the present study, we note that our models agree with the previous studies over the U.S. (Kazil et al., 2014; Luecken et al., 2010), China (Wang et al., 2018), and Europe (Henne et al., 2012). Figure 4 shows the comparison of annual mean (a) TFA deposition (dry and wet combined), and (b) TFA rainwater concentration over the U.S., China, and Europe. We have normalized the emissions to match those of the previous studies for meaningful comparisons. (The emissions used to compare TFA from the U.S., China, and Europe are 24.5, 42.7, and 19.2 Gg yr^{-1}, respectively.) We note that average deposition rates differ in the model because of the differences in calculations' domain sizes. Given that the models vary in their versions, meteorology, physics, and the expected model variabilities, the observed agreement is reasonable. The TFA rainwater concentration in China is a factor of two higher in WRF-Chem because the total precipitation amounts were factors of 1.5-2 higher in GEOS-Chem compared to WRF and TRMM as mentioned in section 3.1. We also show the comparison with our calculations over the U.S. for the summer months with previous studies (Kazil et al., 2014; Luecken et al., 2010; Wang et al., 2018) (Figure S7 in the supplementary information).

3.3. Atmospheric mixing ratios

Figure 5 shows the annual mean mixing ratios of HFO-1234yf over India, China, and the Middle East as simulated by GEOS-Chem and WRF-Chem. We present here only results with emissions in GEOS-Chem(WRF-Chem) of 41.3(41.9), 40.6(39.9), and 37.8(38.1) Gg yr^{-1} from India, China, and the Middle East, respectively. Expected TFA for other emissions can be simply scaled to the emissions of interest. The annual mean mixing ratio of HFO-1234yf in India, China, and the Middle East as simulated by GEOS-Chem(WRF-Chem) were 2.87(3.94) ppt, 2.49(3.70) ppt, and 1.82(2.49) ppt, respectively, and below 1 ppt (as seen in GEOS-Chem) outside of the three regions. The annual mean mixing ratio in the China domain was comparable to Wang et al. (2018). The highest (>40 ppt) simulated annual mean HFO-1234yf mixing ratio for India was in the Indo-Gangetic Plain (IGP), for China in the northeast region, and for the Middle East in northern Iran. The emission hotspots (Figure S1 in the supplementary information) in the three regions led to the largest annual mean HFO-1234yf mixing ratios in those regions. The WRF-Chem simulated higher annual mean HFO-1234yf mixing ratios compared to GEOS-Chem. Differences in annual mean HFO-1234yf mixing ratios between models for the same amount of emissions have been reported also by Henne et al. (2012). However, the overall spatial patterns are comparable between GEOS-

387 Chem and WRF-Chem. It should be noted that the change of HFO-1234yf emissions in any of the
388 three regions would change the HFO-1234yf mixing ratio within that region and will have minimal
389 effect on other regions.
390

3.4. TFA deposition

392 GEOS-Chem simulated mean total deposition rates (dry and wet deposition combined) to
393 be 0.874, 0.501, and 0.477 kg km^{-2} yr^{-1}, respectively, in India, China, and the Middle East domains
394 for emissions of 41.3, 40.6, and 37.8 Gg yr^{-1}, respectively. WRF-Chem simulated mean deposition
395 rates (dry and wet) were 0.802, 0.342, and 0.284 kg km^{-2} yr^{-1} in India, China, and the Middle East
396 domains, respectively (Figure S8 in the supplementary information). Figure 6 shows the annual
397 total dry and wet TFA deposition rates in the three domains. The total annual dry deposition in
398 GEOS-Chem and WRF-Chem over the India domain was largest in eastern India and Bangladesh,
399 reaching up to 2 kg km^{-2} yr^{-1}. The wet deposition in the India domain mostly occurred in the
400 Himalayas' foothills, eastern IGP, parts of central India, and southwest India and was >3.5 kg km^2
401 yr^{-1}. In the China domain, the total dry and wet deposition rates in GEOS-Chem and WRF-Chem
402 were highest in southeast China. The total dry deposition rate in the Middle East domain was
403 highest in northern Iran. The wet deposition rate was the largest in parts of Iran, with differences
404 between the models. The wet deposition dominated the total TFA deposition. The combined annual
405 total deposition pattern was similar to that of wet deposition in the three domains (Figures 6 and
406 S8 in the supplementary information). The seasonal total deposition rates of TFA from dry and
407 wet depositions in the three domains are shown in Figure S9 in the supplementary information.
408 The seasonal deposition rates were highest for June-September, June-August, and April-October
409 in India, China, and the Middle East domains, respectively.
410 Figure 7 shows the percentage contribution of dry and wet deposition to total TFA
411 deposition between GEOS-Chem and WRF-Chem in the three domains. It should be noted that the
412 sum of the two (dry and wet) percent contributions do not add up to exactly 100% because of
413 transport in and/or out of the domains. For the total amount of HFO-1234yf emissions mentioned
414 in Figure S1(supplementary information) and discussed in section 2.2, the total TFA deposition
415 (dry and wet combined) in India, China, and the Middle East domains from GEOS-Chem were
416 23.4, 20.5, and 18.7 Gg yr^{-1}, respectively. The total annual dry(wet) deposition amounts account
417 for 21(36)%, 20(31)%, and 20(29)% of the annual emissions of HFO-1234yf in GEOS-Chem. In
418 WRF-Chem, the annual total TFA deposition was 19.4, 12.1, and 9.9 Gg yr^{-1}, respectively, in India,
419 China, and the Middle East domains. The dry(wet) TFA deposition was 10(37)%, 3(23)%, and
420 4(26)% of the emissions in India, China, and the Middle East domains, respectively. Table S2
421 (Supplementary Information) shows the seasonal TFA deposition (dry and wet) calculated from
422 GEOS-Chem and WRF-Chem models in the three domains. The lower TFA deposition in WRF-
423 Chem compared to GEOS-Chem is due to the venting of surface emissions into the free
424 troposphere (Grell et al., 2004; Kazil et al., 2014) that leads to lower dry deposition in WRF-Chem
425 (Figure 7a). The differences in deposition between models can also be attributed to differences in
426 model resolutions, model transport, meteorological conditions (e.g., precipitation), and cloud

427 treatment. These differences highlight the need for multi-model simulations to estimate the likely
428 variation in these parameters.
429   Figure 8 shows the total TFA deposition (dry and wet combined) for the four emission
430 scenarios (Figure 2) calculated from GEOS-Chem and WRF-Chem. Our results show that the
431 differences in the calculated extent of TFA formed and deposited are about a factor of two between
432 the models. In all cases, the computed TFA dry and wet deposition varies linearly with the
433 emissions. Therefore, we can calculate the amounts of TFA formed and deposited for any
434 envisioned emission of HFO-1234yf.
435
3.5.   Rainwater concentrations

437   Figure 9 shows the monthly variation in mean TFA rainwater concentration in the three
438 domains calculated from GEOS-Chem and WRF-Chem. The TFA rainwater concentration also
439 varies linearly with the emissions. Figure 9 shows the following: (a) higher concentrations are to
440 be expected when there is little rain/precipitation (Figure S10 in the supplementary information)
441 to remove TFA. This point has been noted in previous studies (Kazil et al., 2014; Russell et al.,
442 2012; Wang et al., 2018). So, if all the TFA were concentrated into a small amount of rain, the
443 concentrations have to be larger. Such events are infrequent. They are, relative to the rainier
444 regions, more frequent in the Middle East. The large rainwater concentration does not mean that
445 the amount of deposited TFA is larger; (b) The rainwater concentrations varied inversely with the
446 precipitation amount, as seen by comparing the rainwater TFA levels with the total precipitation
447 (Figure S10 in the supplementary information). A clear signal for the rainfall variation was seen
448 over India, where the monsoon season (June, July, August, and a part of September) bring large
449 and almost constant precipitation. This large precipitation makes the TFA rainwater concentrations
450 extremely small. In other words, this is simply a dilution effect; (c) When the rainfall is small,
451 there are considerable variations as one would expect. Lesser total precipitation arises because of
452 fewer showers and often in spatially and temporally sporadic events. So, the concentrations can
453 vary a great deal. This was also evident over China during dry seasons; and (d) the calculated TFA
454 rainwater concentrations were comparable to previous calculations for China (scaled to emissions,
455 Figure 4b). The variation of rainfall amounts and their geographical distribution as climate changes
456 are uncertain, but there are some estimates. For example, Terink et al., (2013) suggest that there
457 could be a ~20% decrease in precipitation over the Middle East region over the next 20 years. A
458 20% decrease in precipitation will correspond to TFA rainwater concentration less than 40 μg L^{-1}
459 (95th percentile). The annual mean precipitation over China is likely to increase; for example,
460 estimates are roughly increases of 0.078 mm d^{-1} in the 2020s and 0.218 mm d^{-1} in 2050s, with
461 larger changes in the summer months (rainy season) (Guo et al., 2017). The projected rainfall
462 changes across the Indian monsoon region could increase by 6% (RCP4.5) and 8% (RCP8.5) in
463 the mid-21st century (Krishnan et al., 2020).
464   It is important to know the regions of high TFA rainwater concentrations. Therefore, we
465 plotted the spatial pattern of annual mean TFA rainwater concentration in the three domains from
466 both models (Figure S11 in the supplementary information). It is noticeable that most of the regions

467 in all three domains did not have high TFA rainwater concentrations. There were some grids with
468 TFA rainwater concentrations that exceeded 50 μg L^{-1} for emissions of ~40 Gg yr^{-1}. The high TFA
469 rainwater concentration seen in the western part of India and China domains is because of input at
470 the lateral boundaries from a global model. As mentioned in section 3.1, the precipitation in GEOS-
471 Chem was higher, resulting in lower TFA rainwater concentration. Focusing on the highest
472 possible rainwater concentrations is misleading since that does not tell us the amount of wet TFA
473 deposition, which is shown in Figure 6. However, it is clear that if the emissions of HFO-1234yf
474 reach the large numbers noted by the IIASA/GAINS model (max HFO, Figure 2d) for 2040, there
475 will be significant areas with larger TFA rainwater concentrations. The wet deposition does not
476 tell the whole story either since a substantial fraction of the rainwater ends up in the oceans every
477 year. The estimation of the TFA retained on land will be critical for further estimating the long-
478 term impact. Such a hydrology study is warranted but beyond the scope of this work.

479 **3.5.1. Comparison of expected TFA rainwater levels with No Observable Effects**
480 **Concentrations**

481 The primary reason for carrying out these calculations was to estimate the potential impact
482 of HFO-1234yf usage in the three regions of the study for the current and future emissions. The
483 effects of interest here are TFA formation from HFO-1234yf and its consequences to human and
484 ecosystem health. Figure 10 shows the mean TFA rainwater concentration for the four emission
485 scenarios calculated from GEOS-Chem and WRF-Chem. In all the scenarios, the annual mean
486 TFA rainwater concentration was well below the no observed effect concentration (NOEC) for
487 aquatic species, which is >10,000 μg L^{-1} (Solomon et al., 2016), with an outlier for the most
488 sensitive alga as 120 μg L^{-1} (Boutonnet et al., 2011). The negligible impact of TFA formation
489 during the atmospheric oxidation of HFCs, HCFCs, and HFOs has been established for some time.
490 The WMO/UNEP Quadrennial Ozone Assessment (2007) concluded that TFA from the
491 degradation of HCFCs and HFCs would not result in environmental concentrations capable of
492 significant ecosystem damage. Hurley et al., (2008) concluded in their study that the products of
493 the atmospheric oxidation of $CF_3CF=CH_2$ will have a negligible environmental impact. Solomon
494 et al., (2016) also concluded in their study that the concentrations of TFA and its salts in the
495 environment that result from degradation of HCFCs, HFCs, and HFOs in the atmosphere do not
496 present a risk to humans and the environment.

497 Neale et al. (2021) have summarized the impact of TFA on human and ecosystem health.
498 Their conclusion suggests that the NOEC on aquatic systems is >10,000 μg L^{-1}. As shown in
499 Figures 9, 10, and S11 (supplementary information), the expected rainwater concentrations are at
500 least two orders of magnitude lower than the NOEC. Also, the rainwater concentrations of TFA,
501 even for the 2040 emissions, are roughly comparable to those currently observed in China (Chen
502 et al., 2019) and about ten times greater than those presently observed over Germany (Freeling et
503 al., 2020). They also note that large TFA concentrations have been observed in people's blood in
504 China with no ill effects on the endpoints measured in that work (Duan et al., 2020).

505 TFA quantities deposited via dry deposition to land and vegetation would be much smaller
506 than those noted in Neale et al. (2021) to have any significant detrimental health effect. Indeed,

507   they note that there are other sources of TFA that are much higher than those expected from HFO-
508   1234yf degradation. Neale et al. (2021) also point out that the TFA deposited to snow in the Arctic
509   would not significantly contribute to marine water bodies even if it all melted down since the
510   volume of the melt would be much smaller than those of the receiving water bodies.

511   Lastly, since TFA can accumulate over land and water bodies, we can estimate the
512   influence of accumulation on the potential future impacts. The total TFA amount in rainfall would
513   not change. However, the amounts in water bodies could increase. For the 20 years modeled here,
514   the total TFA in water bodies would be larger than those observed for 2020 if TFA merely
515   accumulates. It is hard to calculate precisely where the water bodies would accumulate TFA
516   without a hydrological model. However, these values would still be orders of magnitude smaller
517   than the NOEC of >10,000 μg L^{-1}. For example, if all the TFA produced in these regions were to
518   end up in the top 15 meters of the world's oceans, we expect the TFA levels to increase by about
519   0.015 μg L^{-1} by 2040.

520   Based on these observations, and assuming that the NOEC concentration holds, it appears
521   that the TFA from the expected emissions of HFO-1234yf in these three regions would not
522   constitute a health threat to plants or humans (even if we assume that there is no water treatment
523   to remove TFA in drinking water).

524

525   **3.6.   Interannual variability**

526   The model results discussed in the previous sections are for one year, 2015. To assess the
527   influence of interannual variability in meteorology, we simulated the TFA deposition and
528   rainwater concentration for 2016 with the GEOS-Chem model for the total HFO-1234yf emissions
529   described in section 2.2. Figure 11 shows the fraction of TFA in the three domains for 2015 and
530   2016 that is: (a) dry deposited; (b) wet deposited; and (c) the annual mean TFA rainwater
531   concentrations. The total precipitation in both years was comparable (shown in Figure S12 in the
532   supplementary information). The results of our two-year simulations lead us to conclude that the
533   interannual differences are small. Therefore, we suggest that the results of 2015 are applicable
534   going forward to 2040.

535

536   **3.7.   Simultaneous emissions from multiple regions**

537   It is important to note that most TFA is deposited outside of the domains, even though the
538   estimated lifetime of HFO-1234yf is about ten days. Therefore, TFA is dispersed significantly
539   from the source region. Figure 12a shows that roughly 25-50% of the HFO-1234yf emitted from
540   a given region was converted and deposited (via dry and wet deposition) as TFA within the domain
541   (see Figure 1 for domain boundaries). Figure 12b shows the percentage of TFA deposition (dry
542   and wet combined) calculated from GEOS-Chem and WRF-Chem within the three domains over
543   land. The remaining TFA was transported outside the domain. It is difficult to quantify the exact
544   locations of these depositions outside the domain since the concentrations get very small even
545   though in the aggregate that accounts for somewhere between 30% and 45%. The fraction that was
546   deposited within the region of emission was even smaller and ranged between 7% and 27%.

547   Therefore, it can be concluded that a significant fraction ended up in the oceans. This is especially
548   true for India and the Middle East emissions. Interestingly, a substantial amount of the TFA from
549   the Middle East emissions are deposited in the Arabian Sea. Therefore, we conclude that even
550   though HFO-1234yf is short-lived, it is still sufficiently long-lived to travel thousands of
551   kilometers. Such an expectation is in accord with the calculated distances traveled by an airmass
552   for even about 2 m s[1].

553   The deposition outside of the region and domains also means that the emitting regions are
554   not the only area affected by their emission of HFO-1234yf. This is in spite of the relatively short
555   turnover time of HFO-1234yf. (Note: We call this the turnover time because of the way we
556   calculate it in the model.) Since the three countries/regions studied here are adjacent to each other
557   and their domains overlap (Figure 1), it is possible to estimate the impact of the neighbors'
558   emissions on each other. We consider the emissions over the rest of the world (excluding India,
559   China, the Middle East, the US, and Europe) from Fortems-Cheiney et al. (2015) assuming HFC-
560   134a is substituted with HFO-1234yf on a mole-per-mole basis (the maximum likely emissions
561   scenario). Figure S13 in the supplementary information shows the annual spatial distribution of
562   HFO-1234yf emissions from all the regions as simulated in GEOS-Chem. The percentage
563   deposition of TFA (dry and wet combined) from global and regional (individual regions) emissions
564   of HFO-1234yf is shown in Figure 13. The TFA deposition increased by 7-18% in the three
565   domains because of the emissions from its neighbors. Figure 13 suggests that if the entire world
566   switches to HFO-1234yf, the impact of TFA from the near and far neighbors would be noticeable,
567   but still be at most a factor of 2 or 3 larger. Figure S14 in the supplementary information shows
568   the spatial pattern of the annual total TFA via (a) dry and (b) wet deposition rates from global
569   emissions of HFO-1234yf. The dominant TFA deposition regions were most parts of India,
570   southeast China, parts of Iran, and the southern Arabian Sea. We discussed in section 3.5.1 the
571   potential impacts of such a global switch.

572

573   **3.8.   Reaction of TFA with Criegee intermediates**
574   We examined the influence of CI's potential reactions with TFA on its tropospheric levels.
575   We used the CI concentrations in the boundary layer (0-2 km) from Chhantyal-Pun et al. (2017)
576   in GEOS-Chem and simulated the model for seven months (January to July) using 2015
577   meteorology. Figure S15 in the supplementary information shows the mean surface CI
578   concentration for those seven months calculated at 2° x 2.5° spatial resolution. The CI
579   concentrations in the three regions of our study were less than 2500 molecules cm^{-3}. We calculated
580   the percentage decrease in total TFA deposition within the three domains by including the CI
581   chemistry. We assumed at all the CI reactions with TFA have the rate coefficient measured for
582   that of CH$_2$OO with TFA, i.e., $5 \times 10^{-18}T^2 e^{1620/T}$ cm^3 molecules^{-1} s^{-1}. Figure 14 shows the
583   spatial pattern of decrease in total TFA deposition (dry and wet combined) for seven months by
584   including CI reaction with gas phase TFA for emissions of HFO-1234yf by (a) India, (b) China,
585   and (c) the Middle East. In most of the locations within the three domains, the decrease in total
586   TFA deposition was <2.5%. At a few places in southeast Asia (Figure 14a), western China (Figure

14b), and northern Africa (Figure 14c), the TFA deposition decreased by 7-25%. The decrease in TFA deposition due to CI was 0.03, 0.32, and 0.08 Gg (total for seven months) for India, China, and the Middle East domains, respectively. Figure S16 shows the percentage decrease in mean surface TFA mixing ratio by including the reaction of CI with TFA following the emissions of HFO-1234yf emissions from (a) India, (b) China, and (c) the Middle East. The decrease in the mean surface TFA mixing ratio is less than 2% (0.01 ppt). Overall, the impact of CI on TFA deposition/mixing ratio was small in the regions of study.

4.   Summary

We have investigated TFA formation from emissions of HFO-1234yf, its dry and wet deposition, and rainwater concentration over India, China, and the Middle East with GEOS-Chem and WRF-Chem models. We estimated the TFA deposition and rainwater concentrations between 2020 and 2040 for four HFO-1234yf emission scenarios. The models were simulated for a year (2015), with additional 2016 simulations to understand the interannual variability. We also simulated the model using global emissions to assess interregional effects on TFA deposition. The main results of the study are summarized below:

- Using two models at different spatial resolutions helped us assess the variation in model transport, precipitation, and cloud treatment. These variations yield slightly different calculated TFA levels from the emission of HFO-1234yf. Even though there are discernable differences, the overall conclusions are the same and point to this study's robustness.
- The accuracy of the GEOS-Chem model's ability to calculate wet deposition over the regions of interest was tested by comparing calculated sulfate rainwater concentration with observations. The model reproduces well the multiyear sulfate rainwater concentration (-3% to -13% bias) and its spatial variability (R>0.80) in the three domains.
- Our calculated TFA amounts over the U.S., Europe, and China were comparable to those previously reported when normalized to the same emissions.
- The controlling factor for the amount of TFA from HFO-1234yf is its emissions. The uncertainties in the models and chemistry are secondary to the extent of emissions.
- The TFA deposition was largest over eastern India, southeast China, northern Iran, and the southern Arabian Sea. The TFA wet deposition was comparable between the two models.
- There are large variations in TFA rainwater concentrations associated with rainfall extent. The mean TFA rainwater concentration calculated for the four emission scenarios from GEOS-Chem and WRF-Chem was below the no observable effect concentration (NOEC), suggesting the ecological and human health impacts to be not significant.
- With a chemical turnover time of HFO-1234yf of 10 days, its impact is not local and extends well beyond the region of emissions. This study highlights the enhanced TFA formation by the simultaneous use of HFO-1234yf by neighboring regions. If all the Northern Hemisphere countries were to use HFO-1234yf, the impact would be higher by a factor of 2 or 3. However, these amounts are still much lower than the NOEC noted above.

626   •   We estimate that continued use of HFO-1234yf in India, China, and the Middle East are
627   unlikely to lead to detrimental human health effects based on the current understanding of the
628   effects of TFA in water bodies, as summarized by Neale et al. (2021). (Note we do not assume
629   the water is treated specifically to remove TFA before consumption.)
630   •   We note that a hydrology model of the water flow and TFA concentrations in them would be
631   beneficial to quantify the extent of TFA accumulation in pools and flow out to large water
632   bodies.

633

634 **Acknowledgement:**
635 We are grateful to Jan Kazil (NOAA/CSL) and Rajesh Kumar (NCAR) for help with the WRF-
636 Chem. We are thankful to Jared Brewer and Viral Shah for helping with TFA chemistry in GEOS-
637 Chem. We are thankful to Kirpa Ram for providing the sulfate rainwater concentration data over
638 India. We are grateful to Anwar Khan, Rabi Chhantyal Pun, Dudley Shallcross, and Andrew Orr-
639 Ewing for providing their calculated Criegee intermediate concentrations. The work at CSU was
640 funded by the Global Forum for Advanced Climate Technologies. NCAR is supported by the U.S.
641 National Science Foundation. Pallav Purohit and Lena Höglund-Isaksson gratefully acknowledge
642 funding from IIASA and the National Member Organizations that support the institute.

643

644

645 **References**
646 Amann, M., Bertok, I., Borken-Kleefeld, J., Cofala, J., Heyes, C., Höglund-Isaksson, L.,
647 Klimont, Z., Nguyen, B., Posch, M., Rafaj, P., Sandler, R., Schöpp, W., Wagner, F. and
648 Winiwarter, W.: Cost-effective control of air quality and greenhouse gases in Europe: Modeling
649 and policy applications, Environ. Model. Softw., 26, 1489–1501,
650 doi:10.1016/j.envsoft.2011.07.012, 2011.
651 Amos, H. M., Jacob, D. J., Holmes, C. D., Fisher, J. A., Wang, Q., Yantosca, R. M., Corbitt, E.
652 S., Galarneau, E., Rutter, A. P., Gustin, M. S., Steffen, A., Schauer, J. J., Graydon, J. A., St
653 Louis, V. L., Talbot, R. W., Edgerton, E. S., Zhang, Y. and Sunderland, E. M.: Gas-particle
654 partitioning of atmospheric Hg(II) and its effect on global mercury deposition, Atmos. Chem.
655 Phys., 12, 591–603, doi:10.5194/acp-12-591-2012, 2012.
656 Boutonnet, J. C., Bingham, P., Calamari, D., de Rooij, C., Franklin, J., Kawano, T., Libre, J.-M.,
657 McCul-loch, A., Malinverno, G., Odom, J. M., Rusch, G. M., Smythe, K., Sobolev, I.,
658 Thompson, R. and Tiedje, J. M.: Environmental Risk Assessment of Trifluoroacetic Acid, Hum.
659 Ecol. Risk Assess. An Int. J., 5, 59–124, doi:10.1080/10807039991289644, 2011.
660 Burkholder, J. B., Cox, R. A. and Ravishankara, A. R.: Atmospheric Degradation of Ozone
661 Depleting Substances, Their Substitutes, and Related Species, Chem. Rev., 115, 3704–3759,
662 doi:10.1021/cr5006759, 2015.
663 Chen, H., Zhang, L., Li, M., Yao, Y., Zhao, Z., Munoz, G. and Sun, H.: Per- and polyfluoroalkyl
664 substances (PFASs) in precipitation from mainland China: Contributions of unknown precursors
665 and short-chain (C2–C3) perfluoroalkyl carboxylic acids, Water Res., 153, 169–177,
666 doi:10.1016/j.watres.2019.01.019, 2019.
667 Chhantyal-Pun, R., McGillen, M. R., Beames, J. M., Khan, M. A. H., Percival, C. J., Shallcross,
668 D. E. and Orr-Ewing, A. J.: Temperature-Dependence of the Rates of Reaction of Trifluoroacetic

Acid with Criegee Intermediates, Angew. Chemie - Int. Ed., 56, 9044–9047, doi:10.1002/anie.201703700, 2017.

David, L. M., Ravishankara, A. R., Kodros, J. K., Venkataraman, C., Sadavarte, P., Pierce, J. R., Chaliyakunnel, S. and Millet, D. B.: Aerosol Optical Depth Over India, J. Geophys. Res. Atmos., 123(7), 1–16, doi:10.1002/2017JD027719, 2018.

David, L. M., Ravishankara, A. R., Kodros, J. K., Pierce, J. R., Venkataraman, C. and Sadavarte, P.: Premature Mortality Due to PM2.5 Over India: Effect of Atmospheric Transport and Anthropogenic Emissions, GeoHealth, 3(1), 2–10, doi:10.1029/2018GH000169, 2019.

Duan, Y., Sun, H., Yao, Y., Meng, Y. and Li, Y.: Distribution of novel and legacy per-/polyfluoroalkyl substances in serum and its associations with two glycemic biomarkers among Chinese adult men and women with normal blood glucose levels, Environ. Int., 134(105295), doi:10.1016/j.envint.2019.105295, 2020.

Fast, J. D., Gustafson, W. I., Easter, R. C., Zaveri, R. A., Barnard, J. C., Chapman, E. G., Grell, G. A. and Peckham, S. E.: Evolution of ozone, particulates, and aerosol direct radiative forcing in the vicinity of Houston using a fully coupled meteorology-chemistry-aerosol model, J. Geophys. Res. Atmos., 111(D21305), 1–29, doi:10.1029/2005JD006721, 2006.

Fortems-Cheiney, A., Saunois, M., Pison, I., Chevallier, F., Bousquet, P., Cressot, C., Montzka, S. A., Fraser, P. J., Vollmer, M. K., Simmonds, P. G., Young, D., O'Doherty, S., Weiss, R. F., Artuso, F., Barletta, B., Blake, D. R., Li, S., Lunder, C., Miller, B. R., Park, S., Prinn, R., Saito, T., Steele, L. P. and Yokouchi, Y.: Increase in HFC-134a emissions in response to the success of the Montreal protocol, J. Geophys. Res., 120(22), 11,728-11,742, doi:10.1002/2015JD023741, 2015.

Freeling, F., Behringer, D., Heydel, F., Scheurer, M., Ternes, T. A. and Nödler, K.: Trifluoroacetate in Precipitation: Deriving a Benchmark Data Set, Environ. Sci. Technol., 54(18), 11210–11219, doi:10.1021/acs.est.0c02910, 2020.

George, C., Saison, J. Y., Ponche, J. L. and Mirabel, P.: Kinetics of mass transfer of carbonyl fluoride, trifluoroacetyl fluoride, and trifluoroacetyl chloride at the air/water interface, J. Phys. Chem., 98(42), 10857–10862, doi:10.1021/j100093a029, 1994.

Giglio, L., Randerson, J. T. and Van Der Werf, G. R.: Analysis of daily, monthly, and annual burned area using the fourth-generation global fire emissions database (GFED4), J. Geophys. Res. Biogeosciences, 118(1), 317–328, doi:10.1002/jgrg.20042, 2013.

Grell, G. A., Knoche, R., Peckham, S. E. and McKeen, S. A.: Online versus offline air quality modeling on cloud-resolving scales, Geophys. Res. Lett., 31(16117), doi:10.1029/2004GL020175, 2004.

Grell, G. A., Peckham, S. E., Schmitz, R., McKeen, S. A., Frost, G., Skamarock, W. C. and Eder, B.: Fully coupled "online" chemistry within the WRF model, Atmos. Environ., 39, 6957–6975, doi:10.1016/j.atmosenv.2005.04.027, 2005.

Guenther, A.: Erratum: Estimates of global terrestrial isoprene emissions using MEGAN (Model of Emissions of Gases and Aerosols from Nature) (Atmospheric Chemistry and Physics (2006) 6 (3181-3210)), Atmos. Chem. Phys., 7, 4327, doi:10.5194/acp-7-4327-2007, 2007.

Guenther, A. B., Jiang, X., Heald, C. L., Sakulyanontvittaya, T., Duhl, T., Emmons, L. K. and Wang, X.: The model of emissions of gases and aerosols from nature version 2.1 (MEGAN2.1): An extended and updated framework for modeling biogenic emissions, Geosci. Model Dev., 5(6), 1471–1492, doi:10.5194/gmd-5-1471-2012, 2012.

Guo, J., Huang, G., Wang, X., Li, Y. and Lin, Q.: Investigating future precipitation changes over China through a high-resolution regional climate model ensemble, Earth's Futur., 5, 285–303,

doi:10.1002/2016EF000433, 2017.

Henne, S., Shallcross, D. E., Reimann, S., Xiao, P., Brunner, D., O'Doherty, S. and Buchmann, B.: Future emissions and atmospheric fate of HFC-1234yf from mobile air conditioners in europe, Environ. Sci. Technol., 46, 1650–1658, doi:10.1021/es2034608, 2012.

Hodnebrog, Ø., Aamaas, B., Fuglestvedt, J. S., Marston, G., Myhre, G., Nielsen, C. J., Sandstad, M., Shine, K. P. and Wallington, T. J.: Updated Global Warming Potentials and Radiative Efficiencies of Halocarbons and Other Weak Atmospheric Absorbers, Rev. Geophys., 58(3), 1–30, doi:10.1029/2019RG000691, 2020.

Hurley, M. D., Wallington, T. J., Javadi, M. S. and Nielsen, O. J.: Atmospheric chemistry of CF3CF=CH2: Products and mechanisms of Cl atom and OH radical initiated oxidation, Chem. Phys. Lett., 450, 263–267, doi:10.1016/j.cplett.2007.11.051, 2008.

Janssens-Maenhout, G., Crippa, M., Guizzardi, D., Dentener, F., Muntean, M., Pouliot, G., Keating, T., Zhang, Q., Kurokawa, J., Wankmüller, R., Denier Van Der Gon, H., Kuenen, J. J. P., Klimont, Z., Frost, G., Darras, S., Koffi, B. and Li, M.: HTAP-v2.2: A mosaic of regional and global emission grid maps for 2008 and 2010 to study hemispheric transport of air pollution, Atmos. Chem. Phys., 15, 11411–11432, doi:10.5194/acp-15-11411-2015, 2015.

Kanakidou, M., Dentener, F. J. and Crutzen, P. J.: A global three-dimensional study of the fate of HCFCs and HFC-134a in the troposphere, J. Geophys. Res. Atmos., 100(D9), 18781–18801, 1995.

Kazil, J., McKeen, S., Kim, S. W., Ahmadov, R., Grell, G. A., Talukdar, R. K. and Ravishankara, A. R.: Deposition and rainwater concentrations of trifluoroacetic acid in the united states from the use of hfo-1234yf, J. Geophys. Res., 119, 14,059-14,079, doi:10.1002/2014JD022058, 2014.

Khan, M. A. H., Percival, C. J., Caravan, R. L., Taatjes, C. A. and Shallcross, D. E.: Criegee intermediates and their impacts on the troposphere, Environ. Sci. Process. Impacts, 20, 437–453, doi:10.1039/c7em00585g, 2018.

Kotamarthi, V. R., Rodriguez, J. M., Ko, M. K. W., Tromp, T. K. and Sze, N. D.: Trifluoroacetic acid from degradation of HCFCs and HFCs: A three-dimensional modeling study, J. Geophys. Res., 103(D5), 5747–5758, 1998.

Krishnan, R., Sanjay, J., Gnanaseelan, C., Mujumdar, M., Kulkarni, A. and Chakraborty, S., Eds.: Assessment of Climate Change over the Indian Region : A Report of the Ministry of Earth Sciences (MoES), Government of India, Springer Nature., 2020.

Kuhns, H., Knipping, E. and Vukovich, J.: Development of a united states–mexico emissions inventory for the big bend regional aerosol and visibility observational (bravo) study, J. Air Waste Manag. Assoc., 55(5), 677–692, doi:10.1080/10473289.2005.10464648, 2005.

Kumar, R., Naja, M., Pfister, G. G., Barth, M. C., Wiedinmyer, C. and Brasseur, G. P.: Simulations over South Asia using the Weather Research and Forecasting model with Chemistry (WRF-Chem): Chemistry evaluation and initial results, Geosci. Model Dev., 5(3), 619–648, doi:10.5194/gmd-5-619-2012, 2012.

Kumar, R., Barth, M. C., Pfister, G. G., Delle Monache, L., Lamarque, J. F., Archer-Nicholls, S., Tilmes, S., Ghude, S. D., Wiedinmyer, C., Naja, M. and Walters, S.: How Will Air Quality Change in South Asia by 2050?, J. Geophys. Res. Atmos., 123, 1840–1864, doi:10.1002/2017JD027357, 2018a.

Kumar, S., Kachhawa, S., Goenka, A., Kasamsetty, S. and George, G.: Demand analysis for cooling by sector in India in 2027, New Delhi: Alliance for an Energy Efficient Economy., 2018b.

Li, M., Zhang, Q., Kurokawa, J. I., Woo, J. H., He, K., Lu, Z., Ohara, T., Song, Y., Streets, D. G., Carmichael, G. R., Cheng, Y., Hong, C., Huo, H., Jiang, X., Kang, S., Liu, F., Su, H. and Zheng, B.: MIX: A mosaic Asian anthropogenic emission inventory under the international collaboration framework of the MICS-Asia and HTAP, Atmos. Chem. Phys., 17(2), 935–963, doi:10.5194/acp-17-935-2017, 2017.

Liu, H., Jacob, D. J., Bey, I. and Yantosca, R. M.: Constraints from ^{210}Pb and [7]Be on wet deposition and transport in a global three-dimensional chemical tracer model driven by assimilated meteorological fields, J. Geophys. Res. Atmos., 106(D11), 12,109-12,128, doi:10.1029/2000JD900839, 2001.

Luecken, D. J., Waterland, R. L., Papasavva, S., Taddonio, K. N., Hutzell, W. T., Rugh, J. P. and Andersen, S. O.: Ozone and TFA impacts in North America from degradation of 2,3,3,3-tetrafluoropropene (HF0-1234yf), A potential greenhouse gas replacement, Environ. Sci. Technol., 44, 343–348, doi:10.1021/es902481f, 2010.

Myhre, G., Shindell, D., Bréon, F.-M., Collins, W., Fuglestvedt, J., Huang, J., Koch, D., Lamarque, J.-F., Lee, D., Mendoza, B., Nakajima, T., Robock, A., Stephens, G., Takemura, T. and Zhang, H.: Anthropogenic and Natural Radiative Forcing, edited by T. F. Stocker, D. Qin, G.-K. Plattner, M. Tignor, S. K. Allen, J. Boschung, A. Nauels, Y. Xia, V. Bex, and P. M. Midgley, Cambridge University Press, Cambridge, United Kingdom and New York, NY, USA., 2013.

Neale, R. E., Barnes, P. W., Robson, T. M., Neale, P. J., Williamson, C. E., Zepp, R. G., Wilson, S. R., Madronich, S., Andrady, A. L., Heikkilä, A. M., Bernhard, G. H., Bais, A. F., Aucamp, P. J., Banaszak, A. T., Bornman, J. F., Bruckman, L. S., Byrne, S. N., Foereid, B., Häder, D.-P., Hollestein, L. M., Hou, W.-C., Hylander, S., Jansen, M. A. K., Klekociuk, A. R., Liley, J. B., Longstreth, J., Lucas, R. M., Martinez-Abaigar, J., McNeill, K., Olsen, C. M., Pandey, K. K., Rhodes, L. E., Robinson, S. A., Rose, K. C., Schikowski, T., Solomon, K. R., Sulzberger, B., Ukpebor, J. E., Wang, Q.-W., Wängberg, S.-Å., White, C. C., Yazar, S., Young, A. R., Young, P. J., Zhu, L. and Zhu, M.: Environmental effects of stratospheric ozone depletion, UV radiation, and interactions with climate change: UNEP Environmental Effects Assessment Panel, Update 2020, Photochem. Photobiol. Sci., doi:10.1007/s43630-020-00001-x, 2021.

Neu, J. L. and Prather, M. J.: Toward a more physical representation of precipitation scavenging in global chemistry models: Cloud overlap and ice physics and their impact on tropospheric ozone, Atmos. Chem. Phys., 12, 3289–3310, doi:10.5194/acp-12-3289-2012, 2012.

Pandey, A., Sadavarte, P., Rao, A. B. and Venkataraman, C.: A technology-linked multi-pollutant inventory of Indian energy-use emissions: II. Residential, agricultural and informal industry sectors, Atmos. Environ., 99, 341–352, doi:10.1016/j.atmosenv.2014.09.080, 2014.

Papadimitriou, V. C., Talukdar, R. K., Portmann, R. W., Ravishankara, A. R. and Burkholder, J. B.: $CF_3CF=CH_2$ and (Z)-$CF_3CF=CHF$: Temperature dependent OH rate coefficients and global warming potentials, Phys. Chem. Chem. Phys., 10, 808–820, doi:10.1039/b714382f, 2008.

Papasavva, S., Luecken, D. J., Waterland, R. L., Taddonio, K. N. and Andersen, S. O.: Estimated 2017 refrigerant emissions of 2,3,3,3-tetrafluoropropene (HFC-1234yf) in the United States resulting from automobile air conditioning, Environ. Sci. Technol., 43(24), 9252–9259, doi:10.1021/es902124u, 2009.

Pfister, G. G., Avise, J., Wiedinmyer, C., Edwards, D. P., Emmons, L. K., Diskin, G. D., Podolske, J. and Wisthaler, A.: CO source contribution analysis for California during ARCTAS-CARB, Atmos. Chem. Phys., 11, 7515–7532, doi:10.5194/acp-11-7515-2011, 2011.

Purohit, P. and Höglund-Isaksson, L.: Global emissions of fluorinated greenhouse gases 2005-

807 2050 with abatement potentials and costs, Atmos. Chem. Phys., 17, 2795–2816,
808 doi:10.5194/acp-17-2795-2017, 2017.
809 Purohit, P., Höglund-Isaksson, L., Dulac, J., Shah, N., Wei, M., Rafaj, P. and Schöpp, W.:
810 Electricity savings and greenhouse gas emission reductions from global phase-down of
811 hydrofluorocarbons, Atmos. Chem. Phys., 20, 11305–11327, doi:10.5194/acp-20-11305-2020,
812 2020.
813 Rigby, M., Montzka, S. A., Prinn, R. G., White, J. W. C., Young, D., O'Doherty, S., Lunt, M. F.,
814 Ganesan, A. L., Manning, A. J., Simmonds, P. G., Salameh, P. K., Harth, C. M., Mühle, J.,
815 Weiss, R. F., Fraser, P. J., Steele, L. P., Krummel, P. B., McCulloch, A. and Park, S.: Role of
816 atmospheric oxidation in recent methane growth, Proc. Natl. Acad. Sci. U. S. A., 114(21), 5373–
817 5377, doi:10.1073/pnas.1616426114, 2017.
818 Russell, M. H., Hoogeweg, G., Webster, E. M., Ellis, D. A., Waterland, R. L. and Hoke, R. A.:
819 TFA from HFO-1234yf: Accumulation and aquatic risk in terminal water bodies, Environ.
820 Toxicol. Chem., 31(9), 1957–1965, doi:10.1002/etc.1925, 2012.
821 Sadavarte, P. and Venkataraman, C.: Trends in multi-pollutant emissions from a technology-
822 linked inventory for India: I. Industry and transport sectors, Atmos. Environ., 99, 353–364,
823 doi:10.1016/j.atmosenv.2014.09.081, 2014.
824 Solomon, K. R., Velders, G. J. M., Wilson, S. R., Madronich, S., Longstreth, J., Aucamp, P. J.
825 and Bornman, J. F.: Sources, fates, toxicity, and risks of trifluoroacetic acid and its salts:
826 Relevance to substances regulated under the Montreal and Kyoto Protocols, J. Toxicol. Environ.
827 Heal. Part B, 19(7), 289–304, doi:10.1080/10937404.2016.1175981, 2016.
828 Terink, W., Immerzeel, W. W. and Droogers, P.: Climate change projections of precipitation and
829 reference evapotranspiration for the Middle East and Northern Africa until 2050, Int. J.
830 Climatol., 33, 3055–3072, doi:10.1002/joc.3650, 2013.
831 Tilmes, S., Lamarque, J. F., Emmons, L. K., Kinnison, D. E., Ma, P. L., Liu, X., Ghan, S.,
832 Bardeen, C., Arnold, S., Deeter, M., Vitt, F., Ryerson, T., Elkins, J. W., Moore, F., Spackman, J.
833 R. and Val Martin, M.: Description and evaluation of tropospheric chemistry and aerosols in the
834 Community Earth System Model (CESM1.2), Geosci. Model Dev., 8, 1395–1426,
835 doi:10.5194/gmd-8-1395-2015, 2015.
836 Velders, G. J. M., Fahey, D. W., Daniel, J. S., McFarland, M. and Andersen, S. O.: The large
837 contribution of projected HFC emissions to future climate forcing, Proc. Natl. Acad. Sci. U. S.
838 A., 106(27), 10949–10954, doi:10.1073/pnas.0902817106, 2009.
839 Velders, G. J. M., Fahey, D. W., Daniel, J. S., Andersen, S. O. and McFarland, M.: Future
840 atmospheric abundances and climate forcings from scenarios of global and regional
841 hydrofluorocarbon (HFC) emissions, Atmos. Environ., 123, 200–209,
842 doi:10.1016/j.atmosenv.2015.10.071, 2015.
843 Wallington, T. J., Hurley, M. D., Fracheboud, J. M., Orlando, J. J., Tyndall, G. S., Sehested, J.,
844 Møgelberg, T. E. and Nielsen, O. J.: Role of excited CF3CFHO radicals in the atmospheric
845 chemistry of HFC-134a, J. Phys. Chem., 100, 18116–18122, doi:10.1021/jp9624764, 1996.
846 Wang, Z., Wang, Y., Li, J., Henne, S., Zhang, B., Hu, J. and Zhang, J.: Impacts of the
847 Degradation of 2,3,3,3-Tetrafluoropropene into Trifluoroacetic Acid from Its Application in
848 Automobile Air Conditioners in China, the United States, and Europe, Environ. Sci. Technol.,
849 52, 2819–2826, doi:10.1021/acs.est.7b05960, 2018.
850 Wesely, M. L.: Parameterization of Surface Resistances to Gaseous Dry Deposition in Regional-
851 Scale Numerical Models, Atmos. Environ., 23(6), 1293–1304, doi:10.1016/S0950-
852 351X(05)80241-1, 1989.

853   Wiedinmyer, C., Akagi, S. K., Yokelson, R. J., Emmons, L. K., Al-Saadi, J. A., Orlando, J. J.
854   and Soja, A. J.: The Fire INventory from NCAR (FINN): A high resolution global model to
855   estimate the emissions from open burning, Geosci. Model Dev., 4, 625–641, doi:10.5194/gmd-4-
856   625-2011, 2011.
857   WMO/UNEP Quadrennial Ozone Layer Assessment: Scientific Assessment of Ozone Depletion:
858   2006; WMO: Geneva, Switzerland, , 50, 572, 2007.
859   Young, C. J. and Mabury, S. A.: Atmospheric Perfluorinated Acid Precursors: Chemistry,
860   Occurrence, and Impacts, Rev. Environ. Contam. Toxicol. Vol. 208, 1–109, 2010.
861

862 **Tables**

863 **Table 1.** The slope, correlation coefficient (R), intercept (c), mean bias (MB), and the number of

864 points (N) of simulated (GEOS-Chem) and observed sulfate rainwater concentration over the three

865 domains.

Region	Slope	R	c	MB	N
India	0.771	0.816	0.210	-0.255±0.778	54
China	0.799	0.911	0.655	-1.07±2.700	89
Middle East	1.42	0.880	-2.81	-0.187±2.71	5

866

867 **Figures**
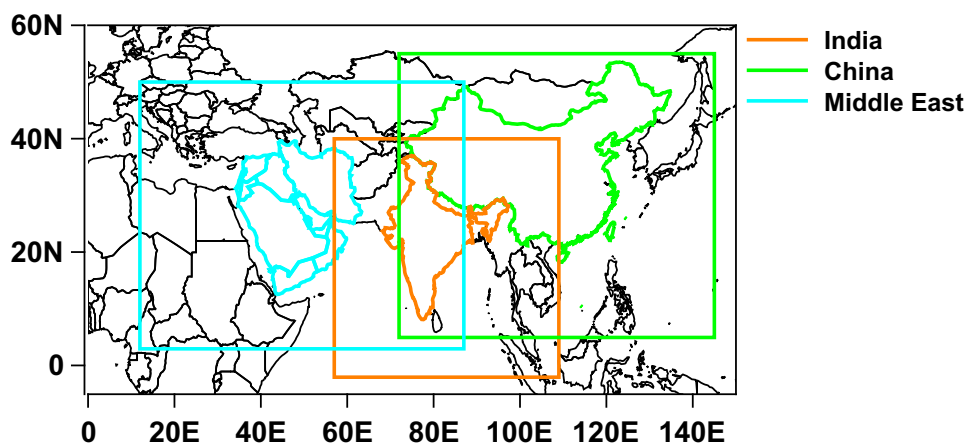
868
869 **Figure 1.** The model domains for India, China, and the Middle East used in the present study and
870 also for WRF-Chem simulations. The land regions for the emissions are shown in color.
871
872
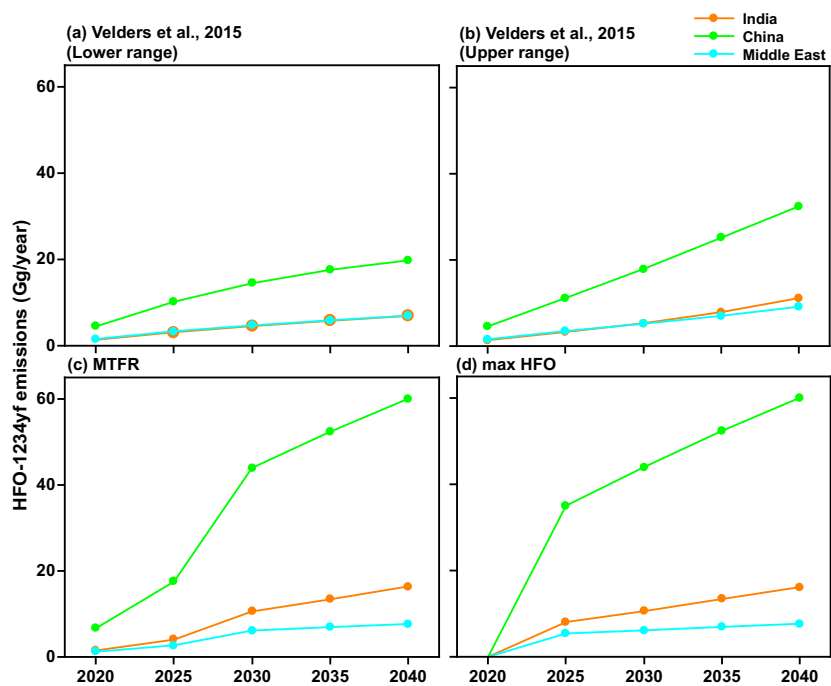
873
874 **Figure 2.** The projected HFO-1234yf emissions scenarios between 2020 and 2040 from Velders
875 et al. (2015) (a) lower and (b) upper ranges, IIASA GAINS model for (c) Maximum Technically
876 Feasible Reduction (MTFR) and (d) max HFO in India, China, and the Middle East.
877
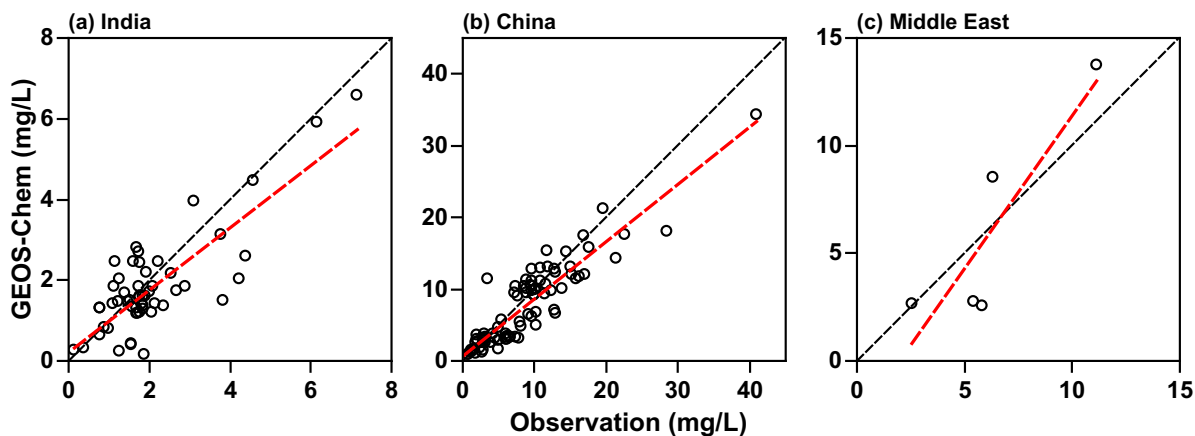
878
879 **Figure 3.** Scatter plot of simulated and observed sulfate rainwater concentration in (a) India, (b)
880 China, and (c) the Middle East for 2000-2015. The linear regression line is shown in red. The black
881 dashed line corresponds to slope = 1. The data for the Middle East is very limited.

882
883
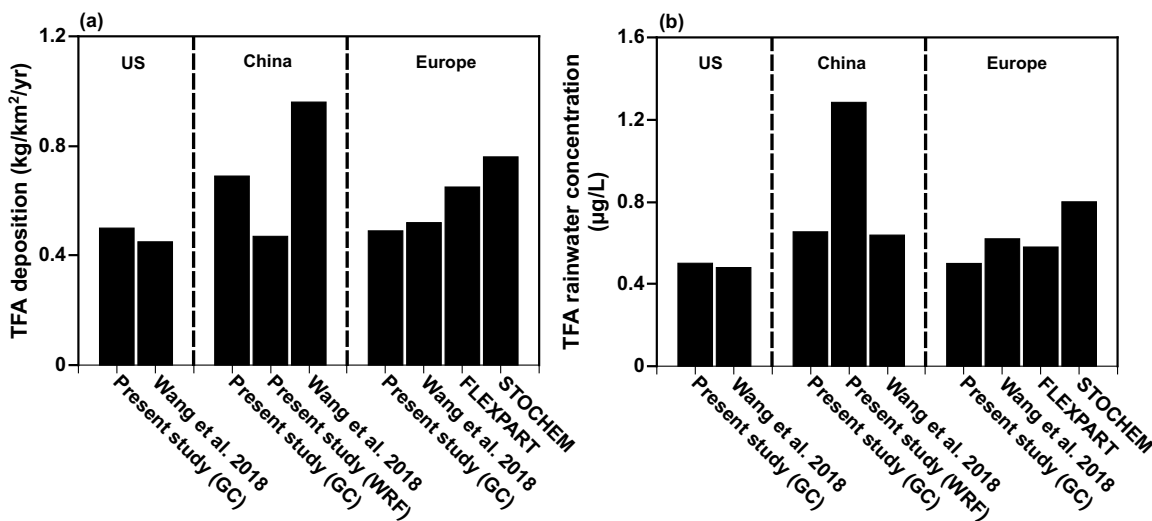
884
885 **Figure 4.** Comparison of the present study with other studies over the U.S., China, and Europe for
886 (a) TFA deposition, and (b) TFA rainwater concentration. Note the emissions are 24.53 Gg yr^{-1},
887 42.65 Gg yr^{-1}, and 19.16 Gg yr^{-1} for the U.S., China, and Europe, respectively.

888
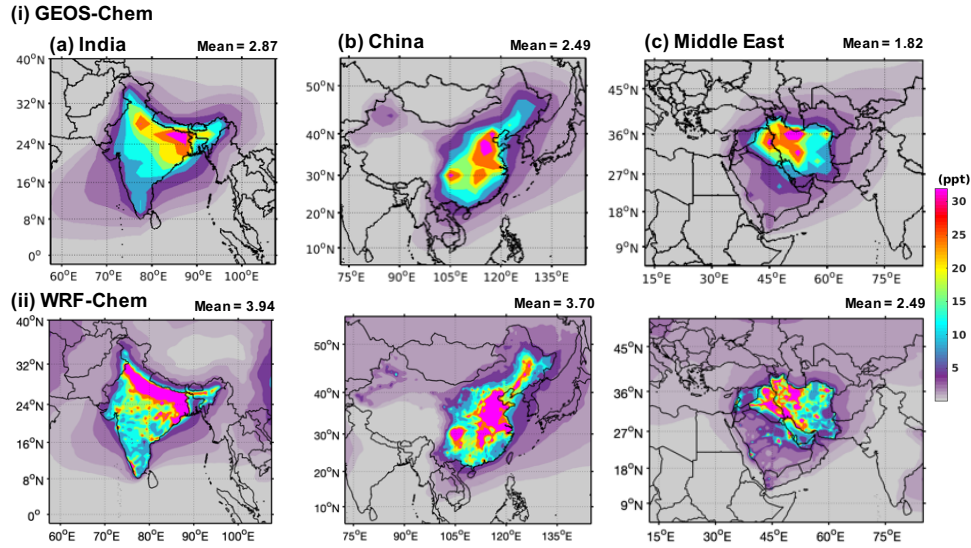
889
890 **Figure 5.** Annual mean surface mixing ratios of HFO-1234yf simulated in (i) GEOS-Chem and
891 (ii) WRF-Chem over (a) India, (b) China, and (c) the Middle East. The number at the top of each
892 panel gives the mean HFO-1234yf mixing ratios within the domains.
893
894
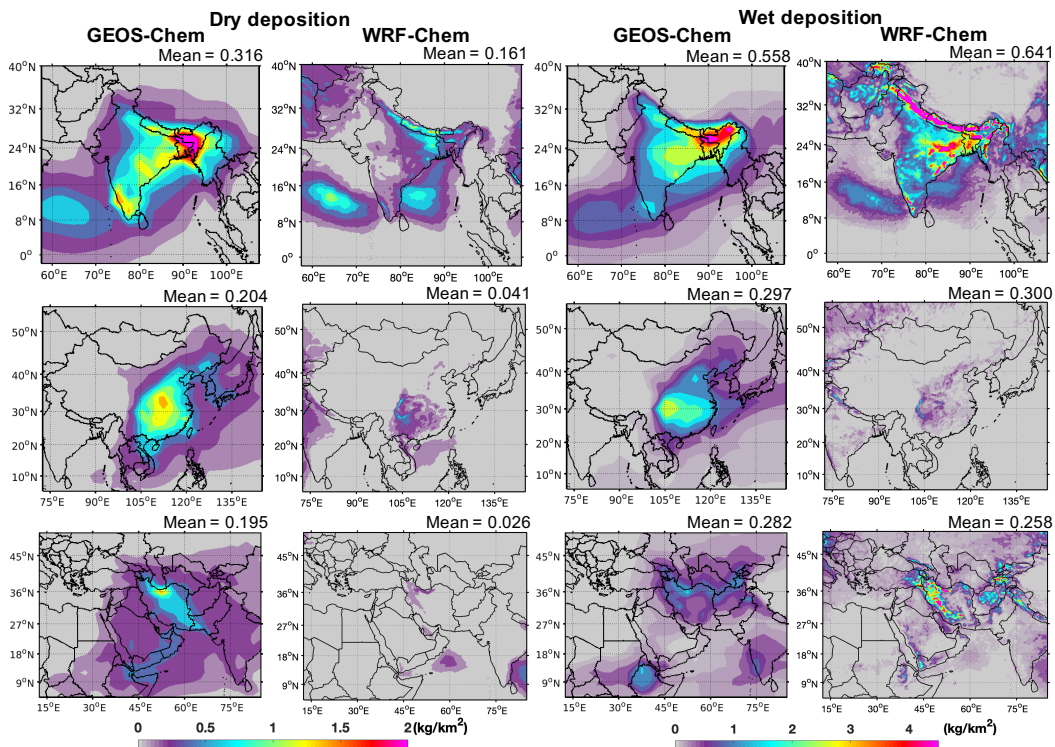
895
896 **Figure 6.** GEOS-Chem and WRF-Chem simulated annual total deposition rates of TFA (kg km^{-2}
897 yr^{-1}) from (a) dry and (b) wet deposition in India, China, and the Middle East domains. The number
898 at the top of each panel gives the mean dry and wet deposition rates within the domains.
899
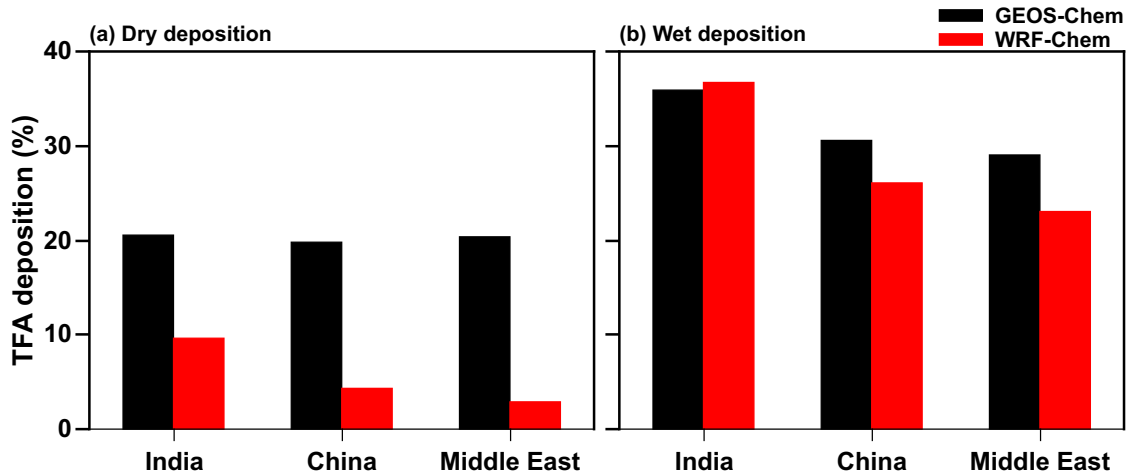
Figure 7. Percentage contribution of (a) dry and (b) wet deposition to total annual TFA deposition simulated in GEOS-Chem and WRF-Chem in the three domains.
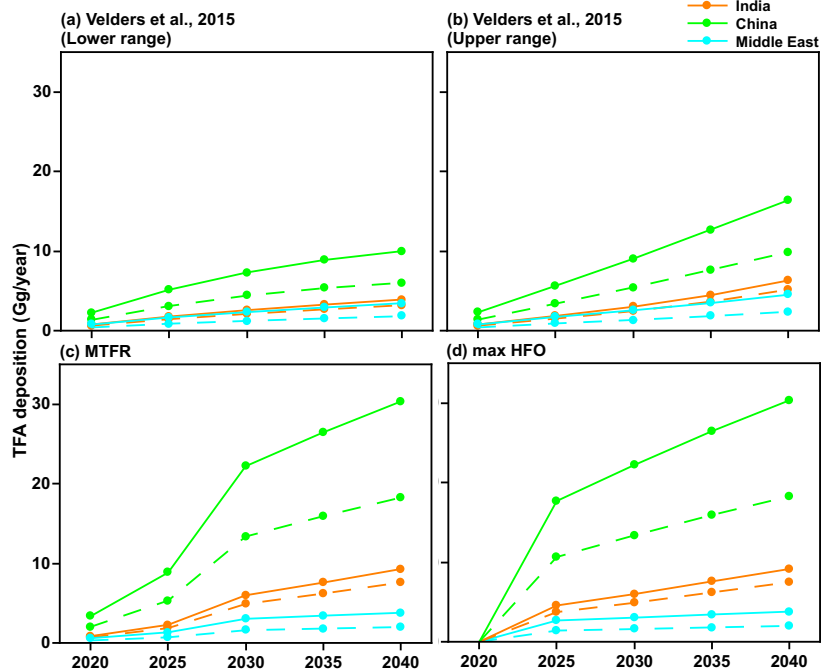
Figure 8. Total TFA deposited (dry and wet combined) in four emission scenarios for 2020 to 2040 within India, China, and the Middle East domains calculated using GEOS-Chem (solid lines) and WRF-Chem (dashed lines). The values from the two models are reasonably close for India and the Middle East, while they differ by almost a factor two for China.
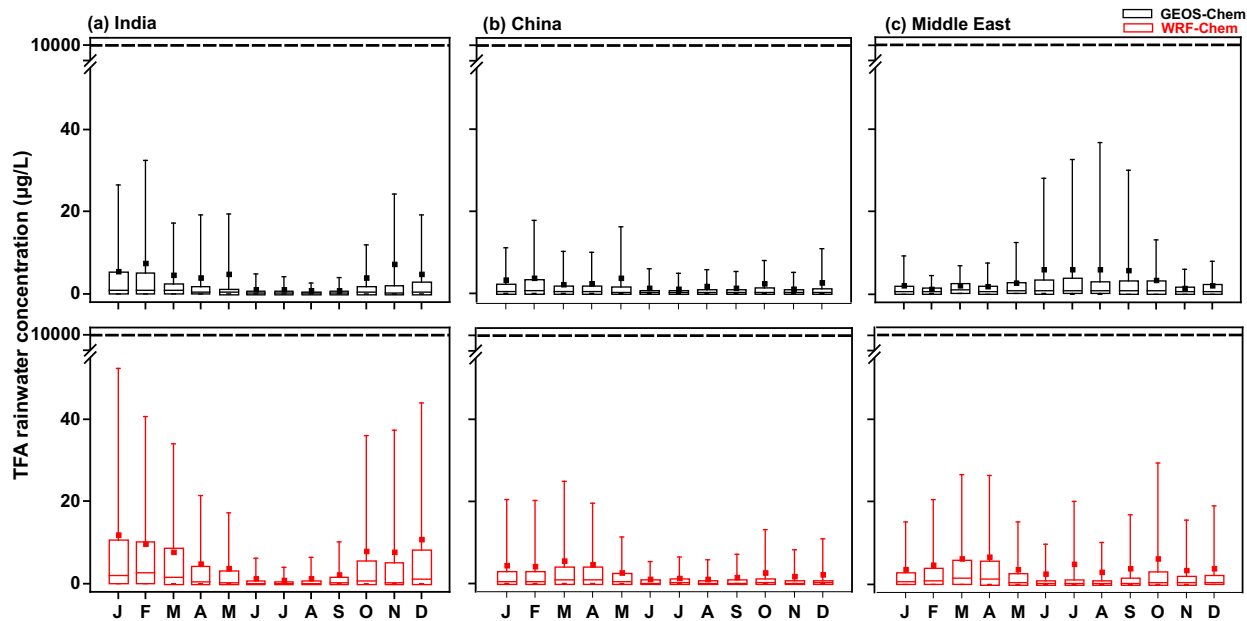
Figure 9. Box and whisker plot of TFA rainwater concentration calculated from GEOS-Chem and WRF-Chem in the three domains. In the box plot, the inside line and square are the median and mean, respectively. Box boundaries are 25th and 75th percentiles, and whiskers indicate the 5th and 95th percentiles. The dashed horizontal line is the No Observable Effect Concentration (NOEC) level. It is important to note that these values, including the 95th percentile values are at least 100 times lower than the NOEC for harming aquatic bodies even when normalized for higher projected emissions in 2040.
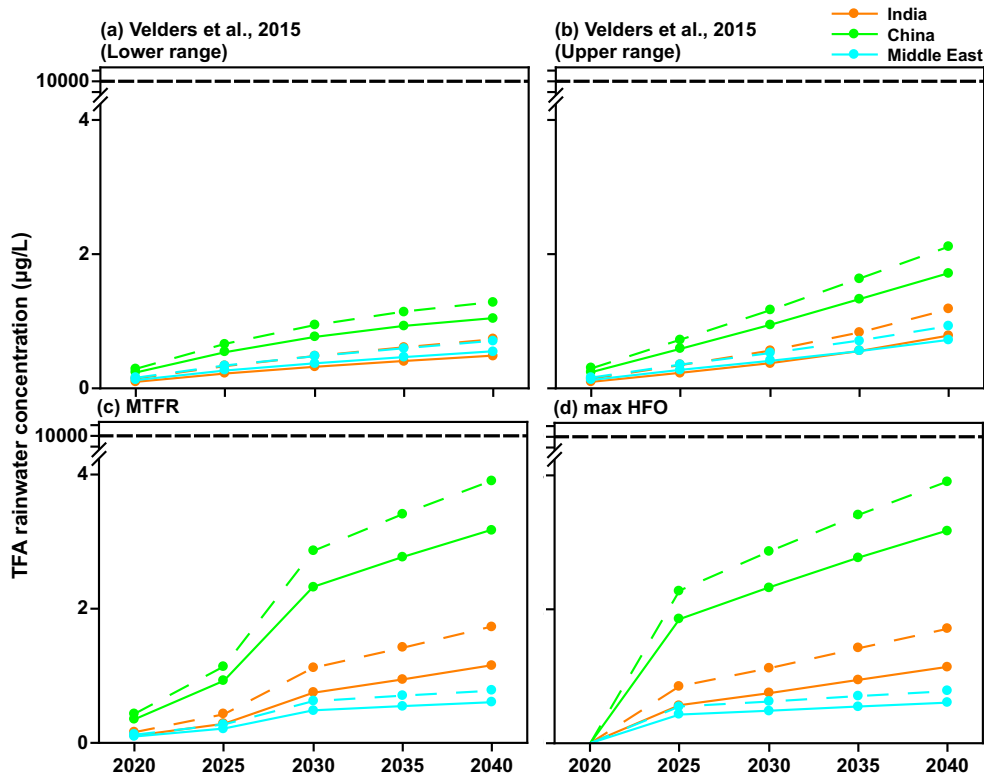
Figure 10. Mean TFA rainwater concentration in four scenarios for 2020 to 2040 for India, China, and the Middle East domains calculated using GEOS-Chem (solid lines) and WRF-Chem (dashed lines). The NOEC is denoted above, and it is two orders of magnitude larger than calculated TFA concentrations for any of the scenarios.
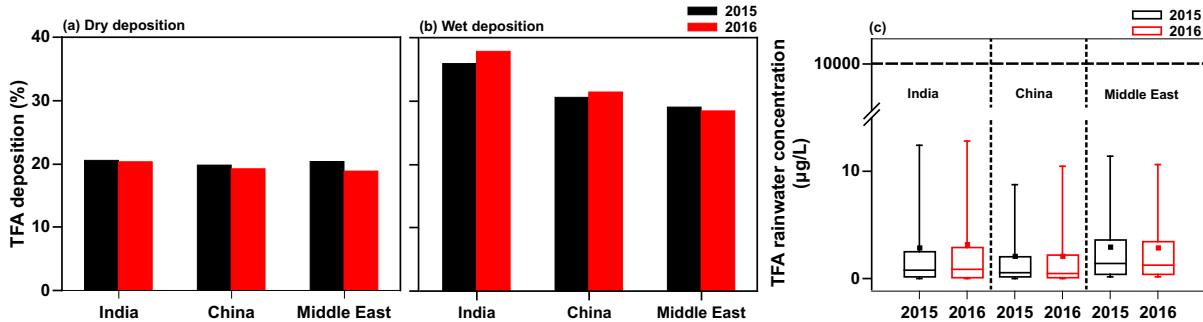
Figure 11. Annual percentage of total TFA (a) dry and (b) wet deposition, and (c) annual mean TFA rainwater concentrations in India, China, and the Middle East domains from GEOS-Chem for 2015 and 2016. The dashed horizontal line is the NOEC level.
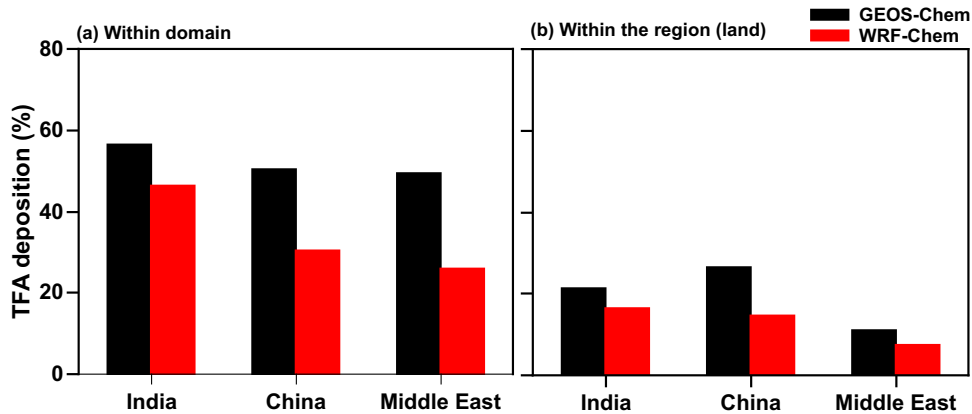
930

931 **Figure 12.** Annual percentage of total TFA deposition (dry and wet combined) calculated from
932 GEOS-Chem and WRF-Chem within the three (a) domains and (b) regions (land).

933
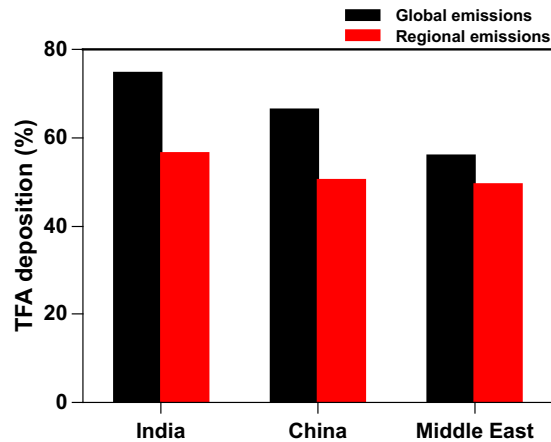
934

935 **Figure 13.** Annual percentage of total TFA deposition (dry and wet combined) in India, China,
936 and the Middle East from global and regional (individual regions) emissions.

937
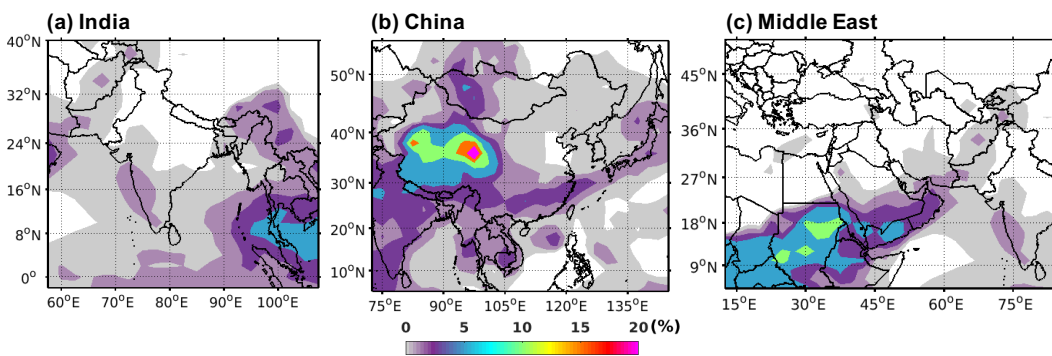
938

939 **Figure 14.** Percentage decrease in TFA deposition (dry and wet combined) by adding Criegee
940 intermediate chemistry to HFO-1234yf emissions over (a) India, (b) China, and (c) the Middle
941 East domains.

942